Unified explanation for linear and nonlinear optical responses in β-carotene: A sub-20–fs degenerate four-wave mixing spectroscopic study

Mitsuru Sugisaki, Kazuhiro Yanagi, Richard J. Cogdell, and Hideki Hashimoto

Unified explanation for linear and nonlinear optical responses in β-carotene: A sub-20-fs degenerate four-wave mixing spectroscopic study

Mitsuru Sugisaki,[1,*] Kazuhiro Yanagi,[2] Richard J. Cogdell,[3] and Hideki Hashimoto[1,†]
[1]*Graduate School of Science, Osaka City University, 3-3-138 Sugimoto, Sumiyoshi, Osaka 558-8585, Japan*
[2]*Nanotechnology Research Institute, National Institute of Advanced Industrial Science and Technology, 1-1-1 Higashi, Tsukuba, Ibaraki 305-8562, Japan*
[3]*Division of Biochemistry and Molecular Biology, IBLS, University of Glasgow, Glasgow, G12 8QQ Scotland, United Kingdom*
(Received 13 December 2006; revised manuscript received 19 February 2007; published 20 April 2007)

The four-wave mixing signal of β-carotene measured under the resonant excitation is reported. A clear coherent oscillation with a period of a few tens of femtoseconds was observed. We have estimated the line broadening function required to simulate this oscillation behavior. The parameters, including the solvation effect, which are essential for calculating the optical signals have also been determined. The validity of our simulation has been evaluated by comparing the theoretically calculated linear and nonlinear optical signals with the experimental results. It was found that in addition to the C—C and C=C stretching modes the methyl in-plane rocking mode significantly contributes to the optical responses of β-carotene. Calculations based on the Brownian oscillator model were performed under the impulsive excitation limit, and we find that the memory of the vibronic coherence generated in the S_2 state is lost via relaxation processes, which include the S_1 state. Comparison between the simulation and experiment revealed that the two-photon absorption process plays an important role in the very early optical process taking place in β-carotene. The vibronic decoherent time of the system is estimated to be 1 ps, which is about five times longer than the population lifetime of the S_2 state determined in the previous studies. The possible relationship between the lifetime of the vibronic coherence and the efficient energy transfer in light-harvesting antenna complexes is discussed.

DOI: 10.1103/PhysRevB.75.155110 PACS number(s): 82.53.Kp, 42.65.Re, 63.22.+m, 78.20.Bh

I. INTRODUCTION

The interaction between a material and its surrounding environment is a fundamental topic for physical and chemical investigation. In any real systems, it is very difficult to eliminate the influence of the environment when investigating the intrinsic properties of a material. From the viewpoint of quantum mechanics, when a material is excited the interactions with the environment makes evolution of a quantum system nonunitary and destroys the coherence of the superpositions of the wave functions. This process is known as decoherence and is directly related to energy dissipation in the material. A clear understanding of the behavior of quantum coherence in dissipative environments is therefore of fundamental importance.

The availability of femtosecond pulses allows the use of time-resolved spectroscopic techniques to observe the evolution of spectra in "real time." It is possible therefore to monitor coherently excited microscopic nuclear motions in condensed matter, which take place on ultrafast time scales.[1] In this context, it is to be expected that new spectroscopies that exploit the phase properties of light will provide new insights into how materials interact with their environment. Information about energy flow or relaxation processes in materials can be obtained by observing the dynamics of coherent vibrational motion, i.e., the dynamics of nuclear wave packets.

In the present paper, we describe the results of exciting β-carotene with 10–20 fs excitation pulses. Carotenoids are important photosynthetic pigments and their photochemical reactions are very sensitive to environmental influences. This makes them ideal molecules in which to study nonlinear optical responses. Carotenoids function as important accessory light-harvesting pigments in photosynthesis. They absorb light in the blue-green region of the spectrum and transfer that absorbed energy rapidly and efficiently to bacteriochlorophyll and chlorophyll molecules. There have been many time-resolved experiments that have investigated the singlet-singlet energy transfer reactions between carotenoids and chlorophylls.[2–5] Depending on which carotenoids and which antenna complexes are studied, the efficiency of these energy transfer processes can vary from as low as 30% to as high as almost 100%. There is still considerable uncertainty, however, as to exactly which excited singlet states are involved in these energy transfer reactions. It is clear, nevertheless, that the light-harvesting proteins are able to modulate the excited-state behavior of the bound carotenoids. Therefore, it is important to investigate energy dissipation and decoherence of carotenoids in order to build up a better picture of how these processes may affect photosynthetic light harvesting.

The use of ultrashort optical pulses has enabled the coherent excitation and real-time observation of molecular vibrations in π-conjugated polymers.[6–10] Further, several research groups have successfully reported the coherent control of retinal,[11] β-carotene,[12,13] and peripheral light-harvesting (LH2) antenna complexes.[14] In the most general terms, these experiments optically excite a chromophore and measure the influence of interactions between the chromophore and the surrounding materials, such as the solvent or the protein environment, on the subsequent evolution of the resulting excited states. This evolution can include both oscillatory coherent nuclear motion and incoherent population decay. Energy transfer can affect vibrational coherences through vibronic coupling or electron-phonon interactions, which are

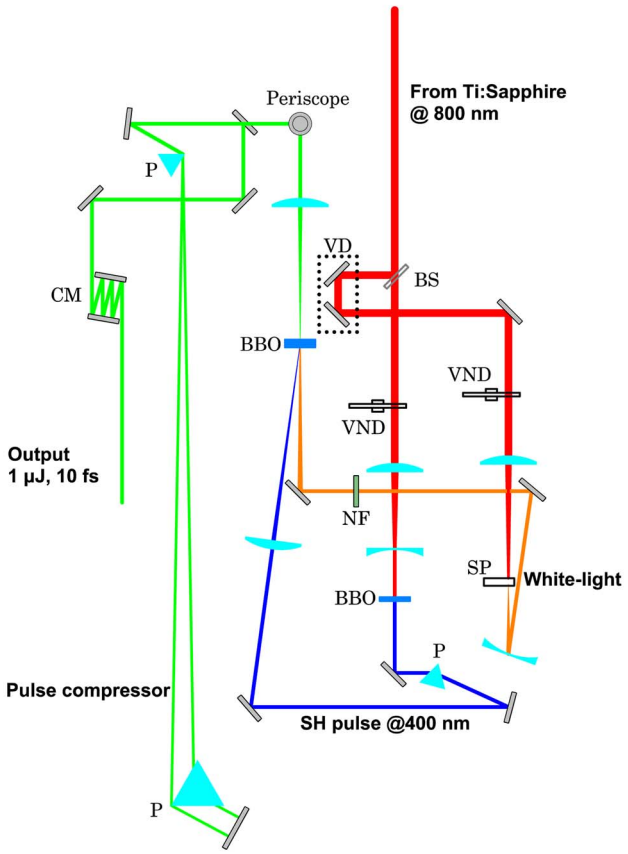

FIG. 1. (Color online) A schematic of the noncollinear optical parametric amplifier (NOPA) and pulse compressor made of a Brewster-cut prism pair and a double chirped mirror. BS: beam splitter, VD: variable optical delay line, VND: variable neutral-density filter, SP: sapphire plate, NF: notch filter, and P: prism.

observable in such ultrafast optical measurements. It is thus essential to investigate the decoherence of vibrational oscillations when discussing the energy dissipation processes of chromophores. Four-wave mixing (FWM) spectroscopy has been reported for β-carotene.[6] In the present paper, we have extended these studies on β-carotene with the aim of producing a detailed comparison between experimental data on coherent oscillations and theoretical model calculations.

II. EXPERIMENTAL DETAILS

A. Construction of a noncollinear optical parametric amplifier system

To produce the excitation light source required for our ultrafast studies, a noncollinear optical parametric amplifier (NOPA) has been constructed. A schematic of the NOPA system is shown in Fig. 1. Initially, a femtosecond Ti:sapphire regenerative amplifier (Spectra Physics, Hurricane) is used to generate 100 fs pulses at 800 nm at a 1 kHz repetition rate. Part of the beam from the amplifier ($\sim$400 μJ) is used for the NOPA system. This beam is then divided into two with a ratio of 9:1. The pump pulses for the NOPA are

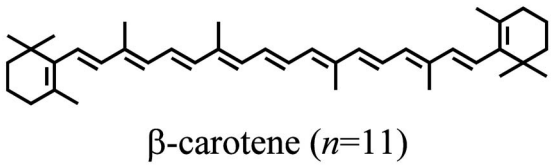

β-carotene (n=11)

FIG. 2. Chemical structure of β-carotene used in the present study, where n indicates the number of conjugated C=C bonds.

obtained by frequency doubling the main fraction of the laser beam in a 400-μm-thick β-BaB_2O_4 (BBO) crystal (type I, θ=29°). The residual of the fundamental laser beam is passed through a delay line for synchronization and then focused onto a 1-mm-thick sapphire plate in order to generate white-light continuum pulses by the self-phase modulation effect. A single filament continuum is used for the seed pulses to produce a stable output of the NOPA. This type of continuum is obtained by carefully adjusting the incident pulse energy so that it is only slightly higher than the threshold required for the white-light continuum generation. It should be noted that the use of a thin sapphire plate is critical in order to generate a flat output from the NOPA with respect to the optical frequency. This is important to be able to compress the pulses effectively. However, the use of *too* thin a plate results in an unstable signal. In this regard, a 1-mm-thick sapphire plate is the optimum choice. In order to further stabilize the NOPA output, we suppressed part of the NOPA spectrum near the fundamental pump beam wavelength by placing a thin bandpass dielectric filter into the seed beam. Parametric gain is achieved in a single path through a 1-mm-thick BBO crystal, cut at θ=31° using the type I phase matching. To minimize the self-focusing effect, the BBO crystal is positioned slightly beyond the focus of the pump beam. The amplified beam, having $\sim$1 μJ in power, is collimated by a spherical lens and then sent to a pulse compressor, made of a pair of Brewster-cut glass prisms. In order to minimize frequency-dependent group delay, a set of chirped mirrors was also employed. By adjusting the insertion of the Brewster prism, the pulse width was optimized. For the measurement of the FWM and six-wave mixing (SWM) signals, the compressed output beam from the NOPA was divided into three using pellicle membranes with a thickness of 2 μm to avoid the additional frequency chirp. The pulse width of the NOPA was measured using a 100-μm-thick BBO crystal. The intensity cross correlation measured between two of the divided beams was better than 10 fs at the best, but typically about 10–20 fs, depending on the central wavelength.

B. Linear and nonlinear spectroscopic studies

The chemical structure of β-carotene used in the present study is shown in Fig. 2. It is a C_{40} hydrocarbon with terminal cyclohexene rings and 11 π-electron conjugated carbon-carbon double bonds. β-carotene was purchased from Wako Pure Chemical Industries, Ltd. and was recrystallized from a benzene solution. For the optical measurements, β-carotene was dissolved in tetrahydrofuran (THF). The optical-

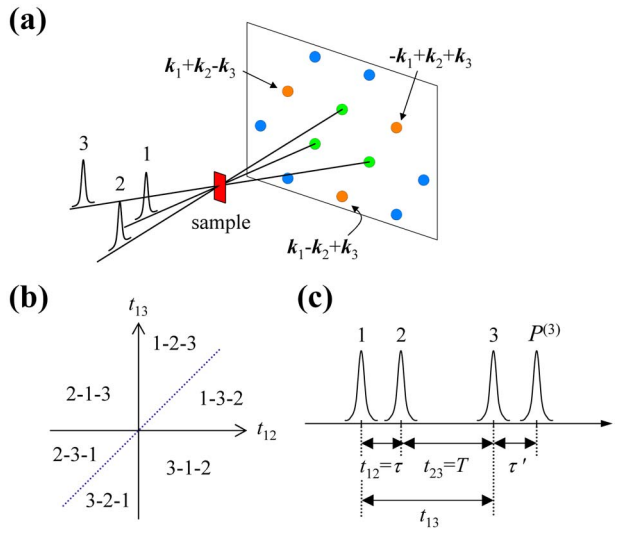

FIG. 3. (Color online) (a) Spatial configuration of the FWM experiment. Three consecutive pulses from the NOPA with wave vectors $\boldsymbol{k}_1$, $\boldsymbol{k}_2$, and $\boldsymbol{k}_3$ are focused in a triangular geometry into the sample. (b) Pulse sequences labeled onto the four quadrants spanned by the time coordinates t_{12} and t_{13}. (c) Time ordering of pulse sequences and notations of time intervals. τ and T denote the center-to-center distances between the pulse pairs (1, 2) and (2, 3), respectively. τ' denotes the delay of the signal from pulse 3.

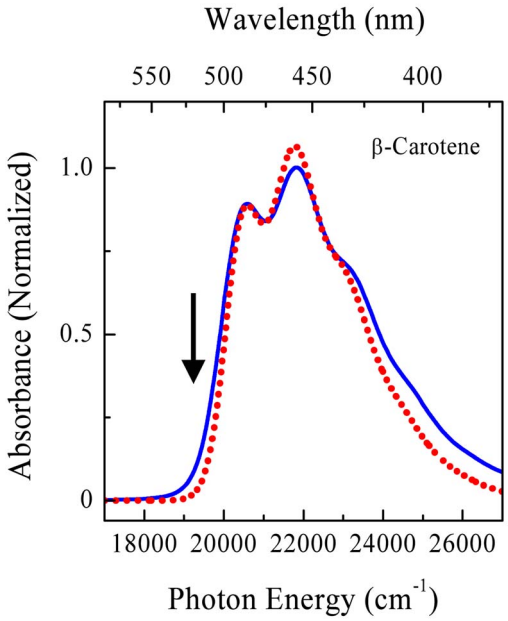

FIG. 4. (Color online) Absorption spectrum of β-carotene. Solid curve: experiment. Dotted curve: simulation calculated using the line broadening function Eq. (1). The arrow indicates the excitation energy for the nonlinear optical measurements.

absorption spectrum was recorded at room temperature in a commercial spectrophotometer (JASCO, V-530).

For the measurement of the Raman spectra, a cw 5 mW He-Ne laser at 632.8 nm was used for the excitation. The signal was resolved using a 30 cm single monochromator (Acton Research, SpectraPro 306i) and then detected by a liquid-nitrogen-cooled charge-coupled device camera (Roper Scientific, LN/CCD-1340/400-EB1).

A 100-μm-thick optical flow cell sandwiched between 1-mm-thick windows was used for the FWM signal measurement in order to minimize possible changes caused by sample degradation. The pulse width was determined by measuring the cross correlations using a 100-μm-thick BBO crystal, where a 1-mm-thick glass plate was placed just in front of the BBO crystal to properly compensate the frequency chirp of the pulses by the window of the flow cell. The pulse width was optimized down to 18 fs at 19 200 cm^{-1} (520 nm), which is near the long-wavelength absorption edge of the sample. The sample concentration was adjusted so that the optical density was $\sim$1 at its absorption maximum.[15] As shown in Fig. 3(a), the three pump pulses in the folded boxcar configuration were focused onto the surface of the sample cell. This configuration was employed in order to separate the signal fulfilling the phase-matching condition from the incoming beams. After passing through the sample, the nonlinear signals were spatially selected using an iris of $\sim$1 mm diameter and then spectrally resolved using a 10 cm single monochromator (JASCO, HR10) with a photomultiplier tube (Hamamatsu, R636-10). The signal was filtered and amplified by means of the lock-in technique.

III. RESULTS AND DISCUSSION

A. Linear absorption spectrum and four-wave mixing signal

The solid curve in Fig. 4 shows the (linear) optical-absorption spectrum of β-carotene in THF. The well-known pronounced structure with an energy spacing of about 1300 cm^{-1} is due to the combination of several vibrational modes. In the absorption spectrum, the dominant band is attributed to the optical transition from the $1\,^1A_g^-$ state (ground state, S_0) to the $1\,^1B_u^+$ state (excited state, S_2). The photoexcitation energy for the nonlinear optical measurements reported below is at 19 200 cm^{-1}, which is indicated by the arrow in Fig. 4. It is at the red edge of the absorption band.

The photograph in Fig. 5 shows the signal taken just behind the sample flow cell. The time delay among all pump beams was set to zero [$t_{12}=t_{13}=0$ (see Fig. 3)]. In addition to the pump-beam spots denoted by the dotted triangle in the middle, the nonlinear signals are clearly observed surrounding them (for more details of this type of nonlinear spectroscopy, see Refs. 16 and 17). The spots marked by the dotted ovals are the so-called FWM signals. Interestingly, the SWM signals are also clearly observed even at room temperature. Some of these are indicated by the arrows. It should be emphasized that these signals, arising from nonlinear interactions up to the fifth order, could be clearly observed by eye. Such higher-order nonlinear signals are usually very faint and difficult to observe. These striking results clearly indicate that carotenoids are very suitable and attractive targets for nonlinear spectroscopy.

Figure 6(a) shows the contour plot of the FWM signal as a function of t_{12} and t_{13}, where t_{12} (t_{13}) is the temporal delay of the pulse 2 (pulse 3) with respect to pulse 1.[18] The exci-

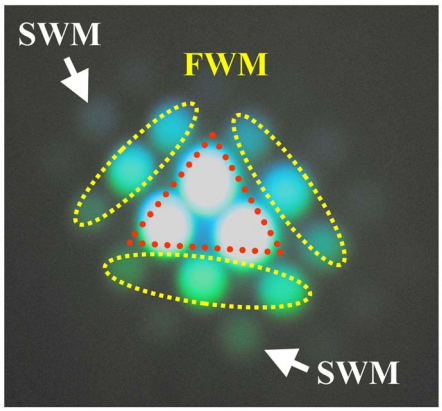

FIG. 5. (Color online) Photoimage of the output signal of the four-wave mixing (FWM) experiment. The third-order optical responses or FWM signals are marked by the dotted ovals. Some of the fifth-order optical responses or six-wave mixing (SWM) signals are indicated by the arrows. The three intense spots in the middle, marked by the triangle, are the pump beams.

tation density of each pulse is about 10 nJ. The corresponding pulse sequences labeled onto the four quadrants spanned by time coordinate t_{12} and t_{13} are shown in Fig. 3.[19] In Fig. 6(a), a very intense signal is observed at the origin of the time axes ($t_{12}=t_{13}=0$), and the transient grating signal is followed along the positive axes of t_{12} and t_{13}. The signal is only observed on these axes and is very weak in the other regions. It should be noted that a coherent oscillation with a period of a few tens of femtoseconds is clearly observed. Also, this contour map is almost symmetrical with respect to the diagonal line $t_{12}=t_{13}$.

We have measured the FWM signals along the three phase-matching directions, i.e., $-\boldsymbol{k}_1+\boldsymbol{k}_2+\boldsymbol{k}_3$, $\boldsymbol{k}_1-\boldsymbol{k}_2+\boldsymbol{k}_3$, and $\boldsymbol{k}_1+\boldsymbol{k}_2-\boldsymbol{k}_3$ [see Fig. 3(a)], where the momentum vector of the ith pulse ($i=1$, 2, and 3) is denoted by $\boldsymbol{k}_i$. In all cases, the

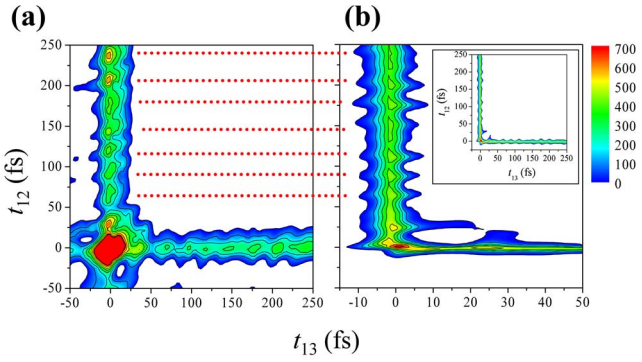

FIG. 6. (Color online) (a) Contour map of the FWM signal observed in the experiment. The signals are almost symmetrical with respect to the diagonal line $t_{12}=t_{13}$. (b) Simulation of the FWM signal calculated under the impulsive excitation condition. The abscissa is magnified because the δ function is assumed for the excitation pulses. The coherent oscillation with a period of 20–30 fs observed in the experimental data is well reproduced by the simulation. The signal calculated over wider temporal region is shown in the inset.

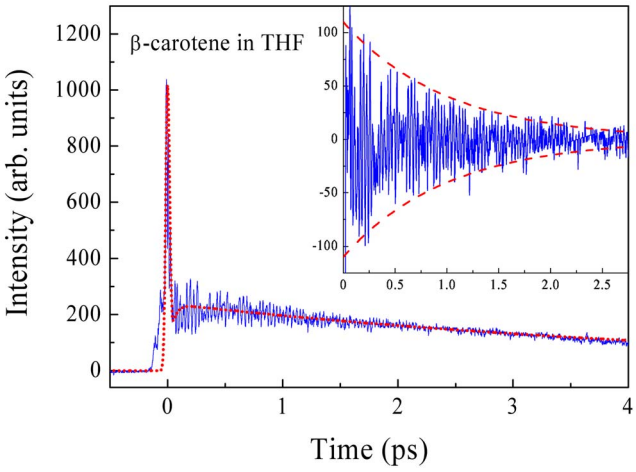

FIG. 7. (Color online) Transient grating signal (solid curve) as a function of the population time t_{13}. The temporal separation of pulses 1 and 2 (t_{12}) was set to zero. The vibronic coherent oscillation is obtained by subtracting the slowly varying background (dotted curve) due to the electronic transition from the solid curve. The residual signal is shown in the inset. The envelope of the coherent oscillation can be well fitted using a single exponential curve, as shown by the dashed curves with a lifetime $\tau_v=1$ ps.

coherent oscillations with a period of a few tens of femtoseconds were clearly observed. In the following, only the results observed along the $-\boldsymbol{k}_1+\boldsymbol{k}_2+\boldsymbol{k}_3$ direction have been analyzed, but all the results can be well accounted for using the same model.

Figure 7 shows the FWM signal of β-carotene that was observed over a wide population period t_{13}. The temporal separation between pulses 1 and 2 (t_{12}) was set to zero; i.e., we focus our attention on the transient grating signal. An intense signal was observed at the $t_{13}=0$. The coherent oscillation with a period of about 20–30 fs is superimposed on a slowly varying component (dotted curve) that decays with a time constant of 4.5 ps. The clear decay profile of the coherent oscillation is observed after the subtraction of the slowly varying component (dotted curve) from the signal, as shown in the inset in Fig. 7. The decay constant of the coherent oscillation can be obtained by fitting a single exponential function $I(t)\propto \exp(-t/\tau_v)$ with a time constant of $\tau_v=1.0$ ps, as shown by the dashed curves.[20]

Figure 8(a) shows the Fourier power spectrum of the oscillations presented in the inset in Fig. 7. For comparison, we also show the Raman spectra of β-carotene (solid curve) and of solvent THF (dotted curve) in Fig. 8(b). The peak energies seen in Figs. 8(a) and 8(b) exactly coincide with each other. We can, therefore, conclude that the coherent oscillation observed in the FWM experiment comes from the molecular vibronic oscillations of β-carotene and the solvent.

We can assign the origin of these vibrations by comparing our results with the resonance Raman spectrum and the normal-coordinate calculations previously performed for *all-trans*-β-carotene.[21] The 1522 cm^{-1} band is due to the symmetric stretch of the C═C bond and the peak at 1157 cm^{-1} can be attributed to the C—C symmetric stretch. In addition to these two most intense bands, the Raman band at

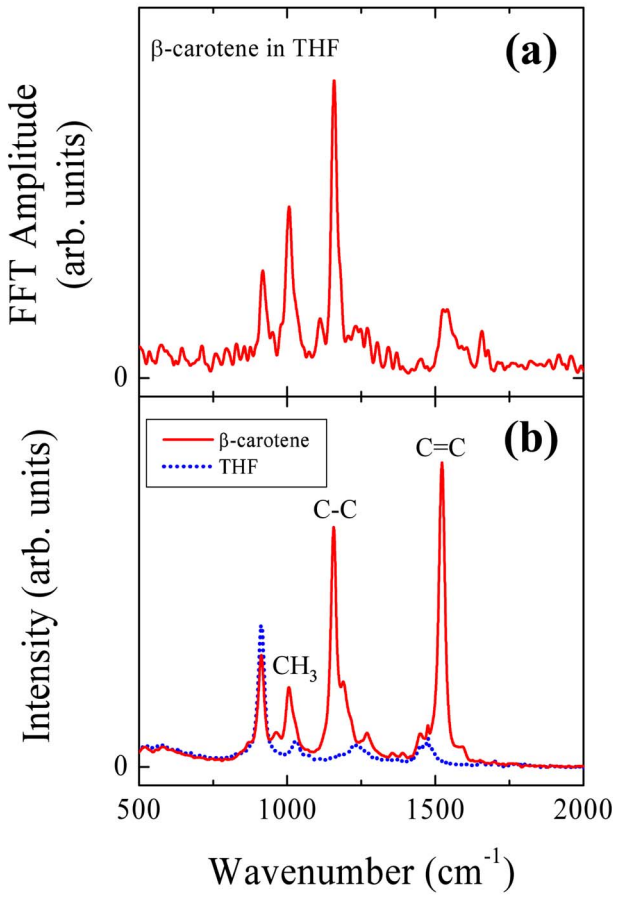

FIG. 8. (Color online) (a) Fourier transform power spectrum of the coherent oscillations shown in the inset in Fig. 7. (b) Raman spectra of β-carotene (solid curve) and solvent (dotted curve) measured with the excitation at 632.8 nm.

1007 cm^{-1} is due to methyl in-plane rocking motions. These three modes have to be taken into consideration as dominant components, when trying to analyze both the linear and nonlinear optical responses from β-carotene. We note that the peak at 912 cm^{-1} comes from the solvent (THF).

B. Numerical calculation

From the viewpoint of nonlinear optics, any time-domain or frequency-domain spectroscopic signal can be calculated using a set of the response functions for a small particle. The following calculations are, therefore, based on the basic protocol of quantum optics.[16,17] The response function is obtained by means of a second-order cumulant expansion. However, in order to determine these response functions, evaluation of the line broadening function is required. In this study, the line broadening function was obtained using the method described in Ref. 17, which is based on the Brownian oscillation model.

The line broadening function $g(t)$, which indicates the time evolution of the transition frequency correlation, can be calculated from the spectral density $\rho(\omega)$,[22,23]

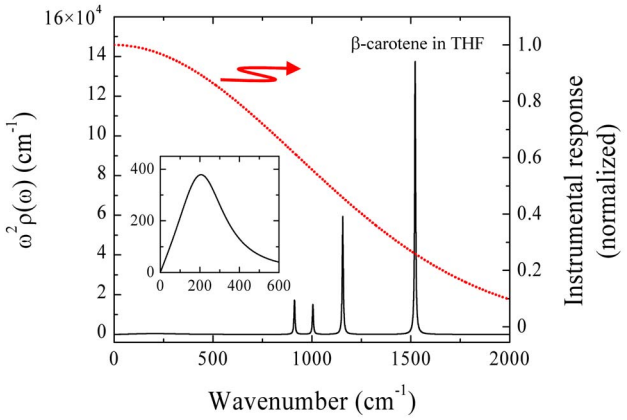

FIG. 9. (Color online) The model spectral density employed for the simulation (solid curve). The inset shows the magnified spectral density assuming a low-frequency Brownian oscillator that represents the influence of the solvent. The instrumental response function (dotted curve) due to the pulse width of 18 fs was determined by the cross correlation measurement.

$$g(t) = -\frac{i\lambda t}{\hbar} + \int_0^\infty d\omega\, \rho(\omega)\coth\left(\frac{\hbar\omega\beta}{2}\right)(1-\cos\omega t) + i\int_0^\infty d\omega\, \rho(\omega)\sin\omega t, \quad (1)$$

where $\beta = 1/k_B T$, k_B is the Boltzmann constant, and T is the temperature. The renormalization constant λ is identical to the solvation reorganization energy,[23,24]

$$\lambda = \hbar\int_0^\infty d\omega\, \omega\rho(\omega). \quad (2)$$

The line broadening function is very important for a description of the optical properties of materials because it contains a complete description of the induced motions, including the amplitudes and time scales.

It should be noted that in some cases, an additional term $(\Delta_{in}t)^2/2$ has to be added to $g(t)$ in order to take into account the inhomogeneous broadening, where Δ_{in} represents the width of the inhomogeneous distribution of the static environment. Here, for simplicity, we have included this in the following way. The low-frequency mode is given by

$$\rho_B(\omega) = \frac{2}{\omega\pi}\frac{\lambda_B\omega_B^2\gamma_B}{(\omega_B^2-\omega^2)^2+\omega^2\gamma_B^2}, \quad (3)$$

which is mainly due to the solvent effect and is given by solving the Langevin equation.[22,25] Here, the subscript B refers to the low-frequency Brownian oscillation mode. In this expression, λ_B, ω_B, and γ_B are the reorganization energy, the frequency of the oscillator, and the damping constant, respectively.

The spectral density used for the following calculation is shown in Fig. 9. We note that the integrated intensity of each peak (area under the curve) represents the Huang-Rhys factor. The line shape of the phonon mode is assumed to be a Lorenzian function.[26] Since the half-width at half maximum

TABLE I. Parameters used for the numerical simulation.

	β-carotene
Δ_{in} (cm^{-1})	0
Γ (cm^{-1})	6
ω_B (cm^{-1})	250
γ_B (cm^{-1})	300
T (°C)	20
λ_B (cm^{-1})	560
ω_{eg} (cm^{-1})	22200
Γ_{20}^{-1} (fs)	1120
Γ_{21}^{-1} (fs)	120
Γ_{10}^{-1} (fs)	9000

of Raman lines shown in Fig. 8 have never been fully determined, we have assumed a value of 6 cm^{-1} for these based on information reported in Ref. 27.

It has been widely accepted that the linear absorption spectrum of β-carotene can be well explained by just the use of two totally symmetric vibrational modes,[28,29] i.e., the C—C ($\hbar\omega_2 \sim 1150$ cm^{-1}) and C=C ($\hbar\omega_3 \sim 1500$ cm^{-1}) stretching modes, even though many other modes can be easily observed in the Raman spectrum. The good agreement between the experiment and calculation is due to a large inhomogeneous broadening Δ_{in}. However, the introduction of methyl in-plane rocking mode ($\hbar\omega_1 \sim 1000$ cm^{-1}) is needed in order to reproduce the nonlinear optical response, which has a significant amplitude as observed in Figs. 8(a) and 8(b). This also means that the methyl in-plane rocking mode plays a significant role in the linear optical spectrum as well. Indeed, several of the parameters obtained by only using two totally symmetric vibrational modes are not so realistic. For example, the displacement of potential minima reported before[28] is about 10% larger than the values obtained in the present study.

The steady-state absorption spectrum of β-carotene can be calculated using the line broadening function as in Eq. (1),

$$\sigma_a(\omega) \propto \mathrm{Re} \int_0^\infty dt \exp[i(\omega - \omega_{eg})t - g(t)], \tag{4}$$

where ω_{eg} indicates the energy separation between the S_0 and S_2 states. The absorption spectrum of β-carotene calculated in this way is shown by the dotted curve in Fig. 4. The parameters used in this simulation are summarized in Table I. The internal conversion rate Γ_{ij} between the S_i and S_j states has been obtained from a recent report by Kosumi *et al.*[30] We note that the homogeneous linewidth of each vibronic oscillation is not sensitive to the shape of the steady-state absorption spectrum.

We now move to the simulation of the FWM signals. To begin with, we tried to calculate the ultrafast optical response of β-carotene by using a simple two-level system, but this was not successful. Instead, we found that the third-order nonlinear optical response can only be described by a modification of the two-state response formalism. Namely, the energy levels that contribute to the optical transition of β-carotene are taken into consideration, and the response functions are then scaled to account for changes in their population.

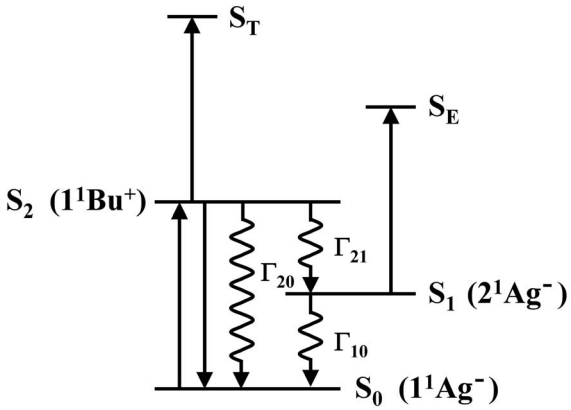

FIG. 10. Schematic energy diagram of β-carotene. Transitions induced by the pump beams are shown by the straight arrows, while the electronic relaxation processes are shown by the wavy lines (internal conversion). S_T and S_E represent the two-photon and excited absorption states, respectively.

Figure 10 shows a schematic energy diagram for β-carotene. The energy diagram of carotenoids is usually described by analogy to *all-trans*-polyenes belonging to the C_{2h} point group.[31,32] Since both the ground state S_0 and the first low-lying excited singlet state S_1 have the same A_g^- symmetry, a one-photon transition between these two states is symmetry forbidden. The lowest optically allowed one-photon singlet state is S_2 and that has B_u^+ symmetry. It should be noted that proposed intermediate states[3,33] between S_1 and S_2 are not included in these calculations, for simplicity. S_E represents the excited state accessed through the $S_n \leftarrow S_1$ absorption process. The final state of a successive two-step absorption process via S_2 state is denoted as S_T (hereafter which is referred to as the two-photon state for simplicity).

The optical responses based on this energy diagram have been calculated using the double-sided Feynman diagrams shown in Fig. 11. The symbols 0, 1, and 2 in these diagrams indicate the S_0, S_1, and S_2 states, respectively. Again, the states which are accessible through the two-photon and excited absorption processes are denoted by the symbols T and E, respectively. The response function formalism for calculating spectroscopic properties of a molecular system from a model of a nuclear dynamics has been extensively discussed.[17,24,34–39] This formalism describes the response of matter to a time-dependent light field and can be used to calculate the third-order nonlinear polarization function. It also allows the ultrafast nonlinear optical responses, such as the three pulse echo peak shift, transient grating, transient absorption signals, and so on, to be calculated (see Ref. 17 and references therein). Similarly, the steady-state absorption and emission spectra can be calculated from the spectral density by this method.

In a simple two-level system, only two processes R_1 and R_2 are counted for calculating the signal in the $t_{12} > 0$ and

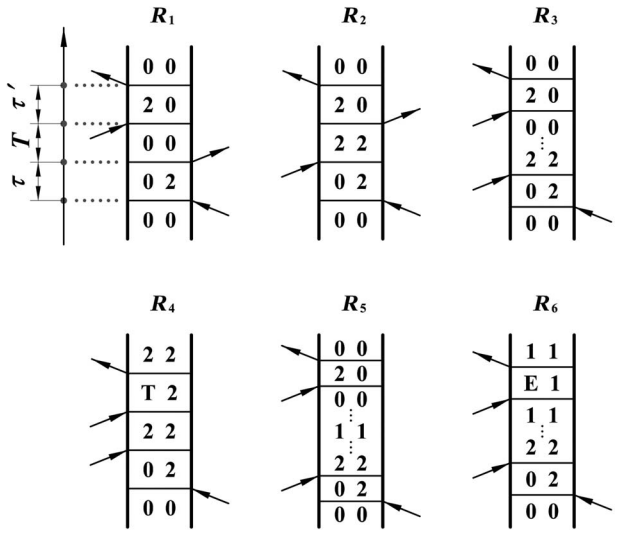

FIG. 11. Double-sided Feynman diagrams that are used for the calculation. The symbols 0, 1, and 2 indicate the S_0, S_1, and S_2 states, respectively. The symbols T and E represent the states S_T and S_E, respectively, as shown in Fig. 10. The time intervals τ, T, and τ' are consistent with those shown in Fig. 3(c). The diagrams R_1 and R_2 are the same as a simple two-level system. The diagram R_3 includes the relaxation directly from S_2 to S_0, while R_5 represents the relaxation from S_2 to S_0 through S_1. The diagram R_4 indicates the two-photon absorption process. The $S_n \leftarrow S_1$ absorption process (so-called "excited-state absorption") is represented in the diagram R_6.

$t_{13} > 0$ region (see Fig. 11). In the present case, however, the description of the nonlinear signal includes four response functions in addition to those of the two-state system, namely, processes R_3 to R_6. Noting that R_3 to R_6 involves an odd number of interactions from the bra side (which gives the negative sign of each response function), the total response function $R(\tau', T, \tau)$ is then obtained by

$$R = R_1 + R_2 - R_3 - R_4 - R_5 - R_6. \tag{5}$$

In order to scale the response functions according to the population kinetics, each response function has to be separated into a nuclear and an electronic population kinetic component.[36–39] Hereafter, the superscript 0 denotes that a separation between the nuclear dynamics and population kinetics has been made.[36] For example, R_2 is scaled as a function of the population time T according to the corresponding kinetics of the S_2 state with the decay rate Γ. For simplicity, we will assume Markovian population kinetics in the following calculation. In this case, we can write $R_2 = R_2^0 e^{-\Gamma T}$.

By referring to Fig. 10, the population change of each state can be obtained by solving a simple set of the following rate equations:

$$\frac{dn_2}{dt} = -(\Gamma_{20} + \Gamma_{21})n_2 \equiv -\Gamma n_2,$$

$$\frac{dn_1}{dt} = \Gamma_{21} n_2 - \Gamma_{10} n_1,$$

$$\frac{dn_0}{dt} = \Gamma_{20} n_2 + \Gamma_{10} n_1,$$

where n_j and Γ_{ij} indicate the population of the jth singlet state S_j and the relaxation rate from the S_i to S_j, respectively. Under the impulsive excitation limit, we obtain

$$n_2(t) = e^{-\Gamma t}, \tag{6a}$$

$$n_1(t) = \frac{\Gamma_{21}}{\Gamma_{10} - \Gamma}(e^{-\Gamma t} - e^{-\Gamma_{10} t}), \tag{6b}$$

$$n_0(t) = \frac{1}{\Gamma_{10} - \Gamma}[(\Gamma_{10} - \Gamma)(1 - e^{-\Gamma t}) + \Gamma_{21}(e^{-\Gamma_{10} t} - e^{-\Gamma t})]. \tag{6c}$$

The population change of the ground state S_0 is affected by two relaxation paths. After the photoexcitation at $t=0$, a part of the population in the S_2 state relaxes through the S_1 state, which is represented in the diagram R_5 (see Fig. 11). The other relaxation path is directly from the S_2 state to S_0, which is represented in R_3. Since the latter case gives the contribution of $r = (1 - \frac{\Gamma 21}{\Gamma})(1 - e^{-\Gamma t})$, R_3 and R_5 may then be written as $R_3 = rR_3^0$ and $R_5 = (n_0 - r)R_5^0$, respectively. The response function R_4 stands for the two-photon process that is very important when considering the ultrafast phenomena of carotenoids.[40] In this process, since the first two pump pulses induce the population in the S_2 state, the response function is scaled by $e^{-\Gamma t}$. The resulting expressions for the response functions are finally obtained using a second-order cumulant expansion,

$$R_1 = |\mu_{20}|^4 \exp[-g^*(\tau) + g^*(T) - g(\tau') - g^*(\tau + T) - g^*(T + \tau') + g^*(\tau + T + \tau')], \tag{7a}$$

$$R_2 = |\mu_{20}|^4 n_2 \exp[-g^*(\tau) + g(T) - g^*(\tau') - g^*(\tau + T) - g(T + \tau') + g^*(\tau + T + \tau')], \tag{7b}$$

$$R_3 = |\mu_{20}|^4 r \exp[-g^*(\tau) - g(\tau')], \tag{7c}$$

$$R_4 = |\mu_{20}|^2 |\mu_{T2}|^2 n_2 \exp[-g^*(\tau) - g(\tau')], \tag{7d}$$

$$R_5 = |\mu_{20}|^4 (n_0 - r) \exp[-g^*(\tau) - g(\tau')], \tag{7e}$$

$$R_6 = |\mu_{20}|^2 |\mu_{E1}|^2 n_1 \exp[-g^*(\tau) - g(\tau')], \tag{7f}$$

where μ_{ij} represents the transition dipole interaction between the S_i and S_j states. The notations of time intervals are shown in Fig. 3; i.e., τ and T denote the center-to-center distances between the pulse pairs (1, 2) and (2, 3), respectively. τ' denotes the delay of the signal from pulse 3.

We note that the process R_6 should always be included. However, in the present case, the excitation energy corresponds to an isobestic point; i.e., the energy where the bleaching of the ground state is canceled out by the excited-state absorption. Therefore, we can omit the process R_6. The expressions of the response functions in the negative time region were calculated in a similar manner by properly con-

sidering the pulse sequences [see Fig. 3(b)] and were then included in our calculation, though their total intensity is weak.

In the calculation of the total response function R, it was assumed that the correlation was lost during the relaxation processes. Namely, noting that the correlation is directly related to the line broadening function, time evolution of the line broadening function during the coherent period $g(T)$ has been omitted in the response functions R_3 to R_5 (see Fig. 11).[38] We also performed the calculation assuming the conservation of correlation (results not shown). However, in this case the calculated signals could not reproduce the experimental results. We conclude, therefore, that the dissipation of the coherence in this system mainly occurs by processes such as internal conversion.

In the homodyne detection scheme, the FWM signal S_{FWM} is given by the time-integrated signal along the $\boldsymbol{k}$ direction,

$$S_{\mathrm{FWM}}(\tau,T)=\int_0^\infty dt|P^{(3)}(\boldsymbol{k},t)|^2, \tag{8}$$

with

$$\begin{aligned}P^{(3)}(\boldsymbol{k},t)\propto&\int_0^\infty dt_3\int_0^\infty dt_2\int_0^\infty dt_1\,R(t_3,t_2,t_1)\\&\times\chi(t_3-t_1)E_3(t-t_3)E_2(t+T-t_3-t_2)\\&\times E_1^*(t+T+\tau-t_3-t_2-t_1)\exp[i(\omega_3+\omega_2-\omega_1)t_3\\&+i(\omega_2-\omega_1)t_2-i\omega_1t_1]\end{aligned} \tag{9}$$

and

$$\chi(t)=\exp(-\Delta_{\mathrm{in}}^2t^2/2). \tag{10}$$

Here, $E_j(t)$ denotes the temporal envelope of the jth incident pulse with its mean frequency ω_j. In Eq. (9), the rotating wave approximation has been employed. In order to simplify the following calculation, we also used two additional approximations. Firstly, we assumed that the experiment was performed under degenerate excitation; i.e., the spectral width is not considered. Secondly, the pulses impulsively excite the dipole moments; i.e., a δ function can be assumed for the excitation pulses. Under these conditions, we finally obtain

$$S_{\mathrm{FWM}}(\tau,T)=\int_0^\infty dt|R(t,T,\tau)|^2|\chi(t-\tau)|^2\sim|R(\tau,T,\tau)|^2, \tag{11}$$

since $\chi(t-\tau)\sim\delta(t-\tau)$.

The pulse width of the excitation light was about 18 fs, measured by cross correlation. Due to the uncertainty principle, this corresponds to about 1800 cm^{-1} in the frequency domain. This is in the same energy range as the phonon modes of carotenoids, which play a crucial role in their optical responses. It is clear, therefore, that the instrumental response has to be properly taken into consideration. In performing our calculations, we introduced the instrumental response function with an 18 fs window, as shown by the dotted curve in Fig. 9.

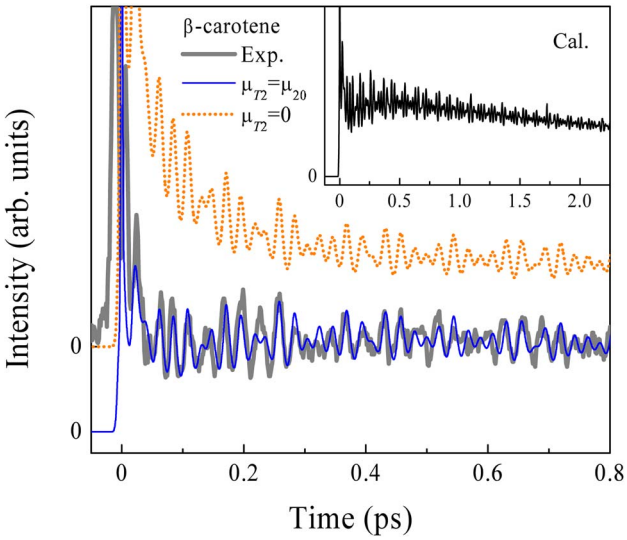

FIG. 12. (Color online) Transient grating signals as a function of the temporal separation of pulses 1 and 3 (t_{13}). The temporal separation of pulses 1 and 2 (t_{12}) was set to zero. Thick solid curve: experimental data. Thin solid curve: theoretical calculation with $\mu_{T2}=\mu_{20}$. For comparison, the signal calculated without including the two-photon process ($\mu_{T2}=0$) is also shown by the thin dotted curve. Inset: transient grating signal calculated over a 2 ps time range.

The contour map calculated, using the spectral density shown in Fig. 9, is presented in Fig. 6(b). The parameters used for the calculation are the same as those used for the calculation of the absorption spectrum (Table I).[41] In Fig. 6(b), the intense signal at the origin is followed by a coherent oscillation, which is the same as the experimental result shown in Fig. 6(a). Further, the calculated coherent oscillation periods exactly match those measured in the experiment.

The transient grating signal ($t_{12}\sim0$) as a function of t_{13} is shown in Fig. 12. The calculation shown by the thin solid curve clearly reproduces the experimental result (thick curve). In Fig. 12, we also show the signal calculated *without* including the two-photon process R_4 (dotted curve). As clearly seen, a fairly good fitting is only obtained when the process R_4 is included. When the two-photon process is not included, the calculated signal in the region of less than 200 fs becomes very large, which is not in agreement with the experimental result. This clearly indicates the importance of the two-photon process in the early stages of the optical response of β-carotene. The close match between our calculations and the experimental results indicates that the spectral density function obtained in the present study accurately reflects the vibronic structure of the system as well as the system-bath interaction.

Kukura *et al.* have recently observed the vibrational spectrum coming from the S_2 state by means of the femtosecond stimulated Raman spectroscopy.[42] They observed high-frequency shifts of the vibrational modes coupled with the S_2 state with respect to those coupled with the S_0 state. In the present study, these high-frequency shifted modes were not considered in the simulation. Nonetheless, the calculated FWM signals together with the transient grating signal agree

very well with the observed results. This means that the spectral density coming from the vibrational modes coupled with the S_2 state has much smaller amplitude compared to those coupled with the S_0 state. At the moment, we consider this as due to the following reason: since the excitation energy is set to the absorption edge, the most dominant process by the first and the second pulses is the 0-0 transition (the transition from the lowest vibrational state of S_0 to that of S_2); i.e., the vibrational modes coupled with the S_2 state are less effectively excited. As mentioned above, in the present model calculation, each response function is separated into a nuclear and an electronic population kinetic component for simplicity. In order to evaluate the spectral density originating from the vibrational modes of the S_2 state, a more detailed theoretical investigation will be required that properly considers this additional vibronic coupling effect. Further, since the expected difference of the oscillation period between the vibrational modes coupled with the S_0 and S_2 states is as small as ~0.2 fs, a much more precise temporal resolution will be necessary, and thus this will be the subject of future work.

It is interesting to compare the lifetime of the coherence seen upon excitation of a carotenoid to the rate of energy transfer from the S_2 and S_1 states to bacteriochlorophyll in purple bacterial LH2 complexes. Energy transfer from the S_2 state typically takes place in less than 100 fs, i.e., well before coherences are lost through the system-bath interaction.[3,5] We suspect that this may be important for the efficient energy transfer from the S_2 state. In contrast, energy transfer from the S_1 state takes place on the same time scale as, or indeed rather longer than, the decay of coherence. It will be interesting, therefore, to investigate whether the loss of coherence affects the efficiency of energy transfer from the S_1 state.

Finally, we briefly comment on the SWM signal. Recently, several groups have reported the SWM signals in various systems, such as atoms,[43] organic molecules,[44] semiconductor quantum structures,[45] and so on.[46] Notably, in some cases, theoretical models have successfully explained these experimental results. The SWM signal of β-carotene is as short as the pulse width of the excitation light source from the NOPA (~20 fs). This means that much shorter optical pulses are necessary in order to get access to the details of such higher order optical processes, which is a challenging but an intriguing subject for a future study.

IV. SUMMARY

In this study, we have successfully measured the FWM signals from β-carotene. Prominent coherent oscillations with a period of a few tens of femtoseconds were clearly observed superimposed on the slowly decaying background that represents the total population dynamics. By comparing the Fourier transformed power spectrum of the coherent oscillations with the Raman spectrum, it is clear that these oscillations mainly come from the C—C and C=C stretching modes and the methyl in-plane rocking mode. The spectral distribution and the line broadening function have been determined, since they are the starting point from which to calculate various kinds of optical spectra. In addition to the linear absorption spectra of β-carotene, the FWM signals have been well reproduced by our calculations. This indicates that the use of the line broadening function that includes both the C—C and C=C stretching modes and the methyl rocking mode is essential for understanding not only the nonlinear optical responses of β-carotene but also the linear optical ones. From the computer simulation, it was confirmed that taking into account the two-photon absorption process is very important for an understanding of the very early events that take place upon excitation of β-carotene. The calculated FWM signal has been well reproduced by assuming decoherence during the relaxation processes between various energy levels of β-carotene. The vibrational decoherence takes place within 1 ps following photoexcitation, which is much longer than the time constant of the energy transfer from the S_2 state of carotenoids to bacteriochlorophyll (~100 fs). This fact may be important for this efficient energy transfer process.

ACKNOWLEDGMENTS

This work was supported in part by the Grant-in-aid from the Japanese Ministry of Education, Culture, Sports, Science, and Technology (Grants No. 17204026, No. 17654083, No. 18340091, and No. 18654074). M.S. also wishes to thank the Shimadzu Science Foundation for financial support. H.H. and R.J.C. thank SICP/JST and the BBSRC (Japan Partnering Award) for financial support. H.H. also acknowledges PRESTO/JST for financial support.

*Corresponding author. Electronic address: mitsuru@sci.osaka-cu.ac.jp

†Electronic address: hassy@sci.osaka-cu.ac.jp

[1] See, for example, R. Leonhardt, W. Holzapfel, W. Zinth, and W. Kaiser, Chem. Phys. Lett. **133**, 373 (1987); S. Ruhman, A. G. Joly, and K. A. Nelson, IEEE J. Quantum Electron. **24**, 46 (1988); R. W. Schoenlein, D. M. Mittleman, J. J. Shiang, A. P. Alivisatos, and C. V. Shank, Phys. Rev. Lett. **70**, 1014 (1993); T. A. Pham, A. Daunois, J.-C. Merle, J. Le Moigne, and J.-Y. Bigot, *ibid.* **74**, 904 (1995); M. Motzkus, S. Pedersen, and A. H. Zewail, J. Phys. Chem. **100**, 5620 (1996); K. D. Rector, A. S. Kwok, C. Ferrante, T. Kokmakoff, C. W. Rella, and M. D. Fayer, J. Chem. Phys. **106**, 10027 (1997); E. J. Brown, I. Pastirk, B. I. Grimberg, V. V. Lozovoy, and M. Dantum, *ibid.* **111**, 3779 (1999); I. Pastirk, V. V. Lozovoy, and M. Dantus, Chem. Phys. Lett. **333**, 76 (2001); G. Cerrulo, J. Lüer, C. Manzoni, S. De Silvestri, O. Shoshana, and S. Ruhman, J. Phys. Chem. A **107**, 8339 (2003); B. E. Prince, A. Chakraborty, B. M. Prince, and H. Stauffer, J. Chem. Phys. **125**, 044502 (2006).

[2] See, for example, A. Angerhofer, R. J. Cogdell, and M. F. Hip-

kins, Biochim. Biophys. Acta **848**, 333 (1986); J. K. Trautman, A. P. Shreve, C. A. Violette, H. A. Frank, T. G. Owens, and A. C. Albrecht, Proc. Natl. Acad. Sci. U.S.A. **90**, 215 (1987); B. P. Krueger, G. D. Scholes, R. Jimenez, and G. R. Fleming, J. Phys. Chem. B **102**, 2284 (1998); J. P. Connelly, M. G. Müller, R. Bassi, R. Crose, and A. R. Holzwarth, Biochemistry **36**, 281 (1997); V. Sundstrom, T. Pullerits, R. van Grondelle, J. Phys. Chem. B **103**, 2327 (1999).

[3] As a review article, T. Polívka and V. Sundström, Chem. Rev. (Washington, D.C.) **104**, 2021 (2004).

[4] P. J. Walla, P. A. Linden, C.-W. Hsu, G. D. Scholes, and G. R. Fleming, Proc. Natl. Acad. Sci. U.S.A. **97**, 10808 (2000); P. J. Walla, J. Yom, B. P. Krueger, and G. R. Fleming, J. Phys. Chem. B **104**, 4799 (2000); P. J. Walla, P. A. Linden, K. Ohta, and G. R. Fleming, J. Phys. Chem. A **106**, 1909 (2002).

[5] Y. Koyama, F. S. Rondonuwu, R. Fujii, and Y. Watanabe, Biopolymers **74**, 2 (2004); F. S. Rondonuwu, K. Yokoyama, R. Fujii, Y. Koyama, R. J. Cogdell, and Y. Watanabe, Chem. Phys. Lett. **390**, 314 (2004).

[6] T. Hornung, H. Skenderović, and M. Motzkus, Chem. Phys. Lett. **402**, 283 (2005).

[7] S. L. Dexheimer, Q. Wang, L. A. Peteanu, W. T. Pollard, R. A. Mathies, and C. V. Shank, Chem. Phys. Lett. **188**, 61 (1992); W. T. Pollard, S. L. Dexheimer, Q. Wang, L. A. Peteanu, C. V. Shank, and R. A. Mathies, J. Phys. Chem. **96**, 6147 (1992).

[8] G. Cerullo, G. Lanzani, M. Zavelani-Rossi, and S. De Silvestri, Phys. Rev. B **63**, 241104(R) (2001).

[9] T. Kobayashi, T. Saito, and H. Ohtani, Nature (London) **414**, 531 (2001).

[10] G. Lanzani, G. Cerullo, C. Brabec, and N. S. Sariciftci, Phys. Rev. Lett. **90**, 047402 (2003).

[11] V. I. Prokhorenko, A. M. Nagy, S. A. Waschuk, L. S. Brown, R. R. Birge, and R. J. D. Miller, Science **313**, 1257 (2006).

[12] J. Hauer, H. Skenderovik, K.-L. Kompa, and M. Motzkus, Chem. Phys. Lett. **421**, 532 (2006).

[13] J. Konradi, A. K. Singh, A. V. Scaria, and A. Materny, J. Raman Spectrosc. **37**, 697 (2006).

[14] J. L. Herek, W. Wohlleben, R. J. Cogdell, D. Zeldler, and M. Motzkus, Nature (London) **417**, 533 (2002); W. Wohlleben, T. Backup, J. L. Herek, and M. Motzkus, ChemPhysChem **6**, 850 (2005).

[15] The optical density (OD) is defined by $\mathrm{OD}=\log_{10} I_0/I$, where I (I_0) is the intensity of the light transmitted in the sample and solvent (solvent only). We note the optical density is not normalized by the thickness of the sample layer.

[16] P. N. Butcher and D. Cotter, *The Elements of Nonlinear Optics* (Cambridge University Press, Cambridge, 1990); R. W. Boyd, *Nonlinear Optics*, 2nd ed. (Academic, Amsterdam, 2003).

[17] S. Mukamel, *Principles of Nonlinear Optical Spectroscopy* (Oxford University Press, New York, 1995).

[18] The relationship between the pulse sequences and spectroscopic techniques is summarized in G. R. Fleming and M. Cho, Annu. Rev. Phys. Chem. **47**, 109 (1996); I. Pastirk, V. V. Lozovoy, and M. Dantus, Chem. Phys. Lett. **333**, 76 (2001); B. I. Grimberg, V. V. Lozovoy, M. Dantus, and S. Mukamel, J. Phys. Chem. **106**, 697 (2002). See also Ref. 17. We note that the contour plot shown in Fig. 6 reflects various kinds of third-order responses since the pulse sequences change as shown in Fig. 3(b). We therefore refer the observed results to as commonly termed FWM signals.

[19] As review articles on transient grating, see M. D. Fayer, Annu. Rev. Phys. Chem. **33**, 63 (1982); **52**, 315 (2001).

[20] We have recently performed the FWM experiment of a β-carotene homolog having 15 π-electron conjugated carbon-carbon double bonds in the same configuration. The decay time τ_v of the coherent oscillation is 1 ps, which is the same as the case of β-carotene. More detailed information will be reported elsewhere.

[21] S. Saito and M. Tasumi, J. Raman Spectrosc. **14**, 299 (1983); S. Saito, M. Tasumi, and C. H. Eugster, *ibid.* **14**, 310 (1983).

[22] W. B. Bosma, Y. J. Yan, and S. Mukame, Phys. Rev. A **42**, 6920 (1990).

[23] Y. J. Yan and S. Mukamel, J. Chem. Phys. **94**, 179 (1991).

[24] M. Cho, J.-Y. Yu, T. Joo, Y. Nagasawa, S. A. Passino, and G. R. Fleming, J. Phys. Chem. **100**, 11944 (1996).

[25] R. Kubo, M. Toda, and N. Hashitsume, *Statistical Physics II: Nonequilibrium Statistical Mechanics* (Springer-Verlag, Berlin, 1991).

[26] R. Jimenez, G. Salazar, J. Yin, T. Joo, and F. E. Romesberg, Proc. Natl. Acad. Sci. U.S.A. **101**, 3803 (2004).

[27] J. Watanabe, S. Kinoshita, and T. Kushida, J. Chem. Phys. **87**, 4471 (1987).

[28] K. Onaka, R. Fujii, H. Nagae, M. Kuki, Y. Koyama, and Y. Watanabe, Chem. Phys. Lett. **315**, 75 (1997).

[29] T. Polívka, D. Zigmantas, H. A. Frank, J. A. Bautista, J. L. Herek, Y. Koyama, R. Fujii, and V. Sundström, J. Phys. Chem. B **105**, 1072 (2001).

[30] D. Kosumi, Y. Yanagi, T. Nishio, H. Hashimoto, and M. Yoshizawa, Chem. Phys. Lett. **408**, 89 (2005).

[31] P. Tavan and K. Schulten, J. Chem. Phys. **85**, 6602 (1986); P. Tavan and K. Schulten, Phys. Rev. B **36**, 4337 (1987).

[32] R. Pariser, J. Chem. Phys. **24**, 250 (1956); P. R. Callis, T. W. Scott, and A. C. Albrecht, *ibid.* **78**, 16 (1983).

[33] As a recent review, H. Hashimoto, K. Yanagi, M. Yoshizawa, D. Polli, G. Cerullo, G. Lanzani, S. De Silvestri, A. T. Gardiner, and R. J. Cogdell, Arch. Biochem. Biophys. **430**, 61 (2004).

[34] S. Mukamel, Phys. Rev. A **28**, 3480 (1983); S. Mukamel and R. F. Loring, J. Opt. Soc. Am. B **3**, 595 (1986).

[35] P. Hamm, M. Lim, and R. M. Hochstrasser, Phys. Rev. Lett. **81**, 5326 (1998); W. P. de Boeij, M. S. Pshenichnikov, and D. A. Wiersma, Chem. Phys. **233**, 287 (1998).

[36] M. Yang, K. Ohta, and G. R. Fleming, J. Chem. Phys. **110**, 10243 (1999).

[37] R. Jimenez and R. E. Romesberg, J. Phys. Chem. B **106**, 9172 (2002).

[38] J. Stenger, D. Dadsen, P. Hamm, E. T. J. Nibbering, and T. Elsaesser, J. Phys. Chem. A **106**, 2341 (2002); E. T. J. Nibbering and T. Elsaesser, Chem. Rev. (Washington, D.C.) **104**, 1887 (2004).

[39] Q.-H. Xu, G. D. Scholes, M. Yang, and G. R. Fleming, J. Phys. Chem. A **103**, 10348 (1999); Q.-H. Xu and G. R. Fleming, *ibid.* **105**, 10187 (2001); Q.-H. Xu, Y.-Z. Ma, and G. R. Fleming, *ibid.* **106**, 10755 (2002).

[40] D. Kosumi, M. Komukai, H. Hashimoto, and M. Yoshizawa, Phys. Rev. Lett. **95**, 213601 (2005).

[41] The parameters listed in Table I may be obtained simply by other spectroscopic techniques, such as stationary absorption spectra and transient absorption change (pump-probe) measurements. One of the advantages of the use of the FWM technique is that γ_B, λ_B, and ω_B are more precisely determined. Namely, when γ_B

is underestimated or λ_B and ω_B are overestimated, peaks along the diagonal line around $t_{12} \approx t_{13} \sim 30$ fs appear in the calculated contour plot, while the calculated absorption spectrum using these inappropriate parameters can reproduce the experimentally observed spectrum. Therefore, the observation of the FWM signal is a better option for the evaluation of these parameters.

[42] P. Kukura, D. W. McCamant, and R. A. Mathies, J. Phys. Chem. **108**, 5992 (2004).

[43] R. Trebino and L. A. Rahn, Opt. Lett. **12**, 912 (1987); G. Gibson, T. S. Luk, A. McPherson, and C. K. Rhodes, Phys. Rev. A **43**, 371 (1991); H. Kang, G. Hernandez, and Y. Zhu, Phys. Rev. Lett. **93**, 073601 (2004); Z. Zuo, J. Sun, X. Liu, Q. Jiang, G. Fu, L.-A. Wu, and P. Fu, *ibid.* **97**, 193904 (2006).

[44] F. Charra, F. Devaux, J.-M. Nunzi, and P. Raimond, Phys. Rev. Lett. **68**, 2440 (1992); K. J. Kubarych, C. J. Milne, S. Lin, V. Astinov, and R. J. D. Miller, J. Chem. Phys. **116**, 2016 (2002); L. J. Kaufman, J. Heo, L. D. Ziegler, and G. R. Fleming, Phys. Rev. Lett. **88**, 207402 (2002); H. Kano and H. Hamaguchi, J. Chem. Phys. **118**, 4556 (2003).

[45] S. R. Bolton, U. Neukirch, L. J. Sham, D. S. Chemla, and V. M. Axt, Phys. Rev. Lett. **85**, 2002 (2000); T. Voss, H. G. Breunig, I. Rückmann, J. Gutowski, V. M. Axt, and T. Kuhn, Phys. Rev. B **66**, 155301 (2002); T. Kishimoto, A. Hasegawa, Y. Mitsumori, J. Ishi-Hayase, M. Sasaki, and F. Minami, *ibid.* **74**, 073202 (2006); V. M. Huxter and G. D. Scholes, J. Chem. Phys. **125**, 144716 (2006).

[46] As a short review, D. S. Chemla and J. Shah, Nature (London) **411**, 549 (2001).